

Structure and Dynamics of Liquid Iron under Earth's Core Conditions

D. Alfè¹, G. Kresse² and M. J. Gillan³

¹*Research School of Geological and Geophysical Sciences
Birkbeck College and University College London*

Gower Street, London WC1E 6BT, UK

²*Institut für Materialphysik, Universität Wien, Strudlhofgasse 4, A-1090 Wien, Austria*

³*Physics and Astronomy Department, University College London
Gower Street, London WC1E 6BT, UK*

First-principles molecular dynamics simulations based on density-functional theory and the projector augmented wave (PAW) technique have been used to study the structural and dynamical properties of liquid iron under Earth's core conditions. As evidence for the accuracy of the techniques, we present PAW results for a range of solid-state properties of low- and high-pressure iron, and compare them with experimental values and the results of other first-principles calculations. In the liquid-state simulations, we address particular effort to the study of finite-size effects, Brillouin-zone sampling and other sources of technical error. Results for the radial distribution function, the diffusion coefficient and the shear viscosity are presented for a wide range of thermodynamic states relevant to the Earth's core. Throughout this range, liquid iron is a close-packed simple liquid with a diffusion coefficient and viscosity similar to those of typical simple liquids under ambient conditions.

PACS numbers: 61.25.Mv, 61.20.Ja 66.20.+d, 71.15.Pd

I. INTRODUCTION

The aim of this work is to use first-principles simulation to determine some of the basic properties of liquid iron at temperatures and pressures relevant to the Earth's core, and to present tests and comparisons which establish the reliability and robustness of the techniques employed. Many lines of evidence show that the Earth's core consists mainly of iron, with a minor fraction of light impurities [1–3]. Since the inner part of the core is solid and the outer part is liquid, a firm grip on the properties of both solid and liquid iron under the relevant conditions is crucial to understanding the behaviour of the core, including its convective dynamics, heat transport, and the generation of the Earth's magnetic field.

The laboratory investigation of iron under core conditions is exceedingly difficult, because of the high pressures and temperatures needed. At the boundary between the mantle and the core, at a depth of ~ 3000 km, the pressure is 135 GPa and the core temperature is believed to be ~ 4000 K [4], while at the boundary between inner and outer core the pressure is 330 GPa and the temperature is thought to be in the region of 5000 K. Experiments using the diamond anvil cell [5–9] can be performed up to ~ 200 GPa, and x-ray diffraction measurements on solid Fe have been made at conditions approaching the core-mantle boundary [8,9]. Beyond this, shock measurements have given some information about the thermodynamic properties of solid and liquid iron [10–12], but the temperature calibration of these measurements is difficult, and there are substantial disagreements between the results. The shear viscosity of the liquid is important for understanding core dynamics, but has been extremely controversial, with estimates

from different sources spanning many orders of magnitude [13,14]. The laboratory measurement of viscosities using the diamond anvil cell is becoming feasible up to pressures of ~ 10 GPa [15,16], but great technical problems still need to be overcome before such measurements can be done under core conditions.

First-principles calculations based on density functional theory (DFT) [17–19] are becoming increasingly important in the study of materials under extreme conditions, and a substantial effort has already been devoted to iron. It is well established that DFT accurately reproduces the properties of low-temperature body-centred cubic (b.c.c.) iron at ambient pressures, including the equilibrium lattice parameter, bulk modulus and magnetic moment [20,21], and phonon frequencies [22]. There has also been much DFT work on different crystal structures of Fe at high pressures, and experimental low-temperature results for the pressure as a function of volume $p(V)$ up to $p = 300$ GPa for the hexagonal close-packed (h.c.p.) structure are accurately predicted [20,21,23]. Further evidence for the accuracy of DFT comes from the successful prediction of the transition pressure from the b.c.c. to the h.c.p. phase [20,23]. Building on these successes, there have been extensive investigations [22,23] of the relative stability and properties of the main candidate crystal structures at pressures up to core values.

Very recently, we have applied the pseudopotential/plane-wave formulation of DFT to calculate the properties of both solid and liquid iron under core conditions [21,24–26]. The great advantage of this DFT formulation is that systems containing tens or hundreds of atoms can be treated. Furthermore, the forces on the atoms are readily calculated, so that dynam-

ical simulations can be performed, and liquids in thermal equilibrium can be simulated. We have reported a brief study of the liquid structure [21], which showed that it is close packed, with a coordination number slightly above 12. We also reported values for the diffusion coefficient, and we used the approximate Stokes-Einstein relation to infer values of the viscosity [24]. Our results indicated that the viscosity of *l*-Fe under core conditions is roughly 10 times greater than that of typical simple liquid metals under ambient conditions. However, our liquid Fe simulations were performed on a very small system of 64 atoms, and we were unable at that stage to investigate system-size errors or errors due to other technical factors such as *k*-point sampling. In addition, we studied only a very small number of thermodynamic states.

Here we report the results of much more extensive first-principles simulations covering a wide range of thermodynamic conditions, and we also describe the thorough study of technical issues that we have now made. An important advance over our previous work is that most of the present calculations are based on the projector augmented wave (PAW) formulation of DFT [27,28]. This is an all-electron technique which is closely related both to other standard all-electron techniques like the linear augmented-plane-wave (LAPW) method [29], and also to the ultrasoft pseudopotential method used in our previous work [21,24–26]. However, in contrast to other all-electron methods, PAW allows one to do dynamical first-principles simulations of the kind that are routinely done with the pseudopotential approach. We report detailed tests on different crystal structures of Fe, which show that the PAW technique reproduces very accurately the available experimental data, as well as the results of previous all-electron calculations. We describe the results of our liquid-state PAW simulations on a range of different system sizes, which allow us to give a quantitative assessment of size errors and other technical factors. A further advance over our earlier work is that we now calculate the viscosity directly from the Green-Kubo relation involving the stress autocorrelation function [30], rather than estimating it from the diffusion coefficient.

Details of our DFT techniques are given in the next Section, and the results of our tests on crystalline iron are reported in Sec. 3. Our detailed tests on the reliability of our techniques for studying the liquid are presented in Sec. 4, where we also report results for the radial distribution function, diffusion coefficient and viscosity of the liquid over a range of conditions. Discussion and conclusions are given in Sec. 5.

II. METHODS

Density-functional theory is a general and extremely widely used set of techniques for treating the energetics of condensed matter, and it has frequently been reviewed

(see e.g. Refs. [18,19,31,32]). Originally formulated as a method for calculating the energy of the electronic ground state of collections of atoms for given nuclear positions [33,34], it was later generalized to calculate the electronic free energy when the electrons are in thermal equilibrium at some finite temperature [35] (again, for given nuclear positions). Since DFT also yields the forces on the nuclei *via* the Hellmann-Feynman theorem, it is also possible to perform first-principles molecular dynamics [17], in which the nuclear positions evolve according to classical mechanics under the action of the forces, while the electronic subsystem follows adiabatically, either in the ground state or in the state of instantaneous thermal equilibrium.

Implementations of DFT can be divided into all-electron (AE) methods, in which both core and valence electrons are treated explicitly, and pseudopotential methods, in which only valence electrons are treated explicitly, their interactions with the cores being represented by a pseudopotential. AE methods, such as the well-known FLAPW (full-potential linear augmented plane-wave) and FP-LMTO (full-potential linear muffin-tin orbitals) schemes, are traditionally regarded as more ‘rigorous’, but at present can be applied only to rather small numbers of atoms, and it is difficult to use them for dynamical simulations. The pseudopotential approach, by contrast, is routinely used for dynamical simulations on systems of tens or hundreds of atoms. First-row and transition-metal elements used to be far more demanding with the pseudopotential approach, but the introduction of so-called ‘ultrasoft’ pseudopotentials (USPP) [36] has largely overcome these problems.

In the last few years, a new method, known as PAW (projector augmented wave) has been developed [27], which effectively bridges the divide between AE and pseudopotential methods. It is an all-electron method, in the sense that it works with the true Kohn-Sham orbitals, rather than orbitals that are ‘pseudized’ in the core regions, and it has the same level of rigor as AE methods such as FLAPW. At the same time, it is very closely related to the USPP technique, and reduces to this if certain well-defined approximations are made, as shown in the recent analysis by Kresse and Joubert [28]. The nuclear forces can be calculated in the same way as in pseudopotential methods, so that dynamical simulations can be performed at essentially the same cost as with the USPP method. An extensive set of comparisons between the PAW, USPP and AE approaches has recently been presented [28] for a variety of small molecules and bulk crystals, including Fe, Co and Ni, and it was shown that the three approaches give virtually identical results in most cases. The only significant exception is ferromagnetic Fe, where fully converged results are easier to obtain with PAW than with USPP. The present work makes direct use of the work of Kresse and Joubert, and was performed with the PAW facility devel-

oped in the VASP code [37,38]. The details of the core radii, augmentation-charge cut-offs etc. in the present PAW work are exactly as in the Fe calculations reported in Ref. [28].

It is known that under Earth’s core pressures it is not accurate enough to neglect the response of the $3s$ and $3p$ electrons to the high compression. The $3p$ response is most significant, and in order to achieve good accuracy we treat both $3p$ and $3d$ as valence electrons. However, this makes it very costly to do long dynamical simulations on large systems, and we showed earlier [21] that it is an accurate approximation to treat the $3p$ orbitals as rigid provided the effect of their response is included by an effective pair potential. (We stress that non-linear core corrections are included everywhere in the present work.) The procedure used to construct this effective potential is as follows (see also Ref. [39]). We calculate the total energies of an perfect h.c.p. Fe crystal in two ways: in the first we include the $3p$ orbitals in valence, and in the second we freeze them in the core. The effective pair potential is then constructed so as to reproduce the difference of the energies between the two sets of calculations. The accuracy of this procedure for treating $3p$ response is demonstrated in Sec. 3 in our comparison of the phonon frequencies of the f.c.c. phase at high pressure. In the following, we refer to calculations in which $3p$ and $3s$ orbitals and below are in the core as ‘Ar-core’ calculations, and those in which $3p$ orbitals are included in the valence set but $3s$ orbitals and below are in the core as ‘Ne $3s^2$ -core’ calculations.

In the temperature range $T > 3000$ K of interest here, thermal excitation of electrons is important, and throughout this work we use the finite-temperature formulation of DFT [35]. This means that each Kohn-Sham orbital has an occupation number given by the usual Fermi-Dirac formula. This thermal excitation has an important effect both on the pressure in the system and on the nuclear forces, as will be reported in detail elsewhere. However, it should be noted that this procedure ignores the possible temperature dependence of the exchange-correlation functional about which little is currently known.

Further technical details are as follows. All the calculations presented here are based on the form of generalized gradient approximation (GGA) known as Perdew-Wang 1991 [40,41]. In the very few spin-polarized calculations we have performed, the spin interpolation of the correlation energy due to Vosko *et al.* was used [42]. Brillouin-zone sampling was performed using Monkhorst-Pack (MP) special points [43]. Most of the dynamical simulations on the liquid were performed using Γ -point sampling only, though we shall report tests using more k -points. The plane wave cut-off was 300 eV in all calculations. The extrapolation of the charge density from one step to the next was performed using the technique described by Alfè [44]. The time-step used in the dynamical

simulations was 1 fs.

III. SOLID IRON

In order to demonstrate the robustness and reliability of the present PAW methods, we have calculated a range of solid-state properties of iron and compared them with experimental values, and with the results of other DFT implementations, including FLAPW, FP-LMTO and ultra-soft pseudopotentials. We also probe the effect of treating the valence-core split in different ways. We have taken pains to ensure that every result given by the present calculations is fully converged with respect to k -point sampling, plane-wave cut-off, and all other technical factors.

In Table I, we report values of the equilibrium volume V_0 for the b.c.c. and h.c.p. structures, the bulk modulus K_0 and its pressure derivative dK_0/dp , and the magnetic moment μ per atom of the (ferromagnetic) b.c.c. phase. In the calculation of K_0 and K'_0 for b.c.c., the moment μ is, of course, free to change with volume. In the h.c.p. case, the equilibrium value of the c/a ratio is determined by minimizing the total energy at fixed volume. Since in principle c/a can depend on volume, this must be taken into account in the calculations of K_0 and K'_0 . In the region of zero pressure we find the value $c/a = 1.58$, which agrees exactly with the calculated value of Ref. [20], and is in reasonable agreement with the experimental values in the range 1.58 – 1.61 reported in Ref. [45]. We note the excellent stability of the results with respect to DFT implementation, and the generally very good agreement with experimental values. We expect the most accurate variant of our PAW calculations to be the one based on the Ne $3s^2$ core, and V_0 values calculated in this way agree with FLAPW values to within 1 % or better. The agreement between PAW[Ne] $3s^2$ and FLAPW results for K_0 and K'_0 is also excellent for h.c.p. . The magnetic moment depends only weakly on the DFT method. The agreement of our PAW results with experimental values is very good for b.c.c., but less good for h.c.p.. However, the experimental values for V_0 and K_0 in the h.c.p. phase do not come from direct measurements at zero pressure (since the h.c.p. crystal is unstable at this pressure), but from an extrapolation from measurements at higher pressures. The reliability of the “experimental” values is therefore not clear.

Our calculated phonon dispersion curves for the zero-pressure b.c.c. phase are compared with experimental frequencies in Fig. 1. The calculations were done using our implementation of the small-displacement method described in Ref. [46]. Small systematic differences can be seen for transverse modes at some wavevectors on the $\Gamma - N$ and $\Gamma - H$ lines, but even at worst these do not exceed *ca.* 10 %.

Fig. 2 compares calculated values for p as a function of V of the h.c.p. crystal with experimental measurements due to Mao *et al.* [45]. On the scale of the Figure, the PAW results obtained with the Ne3s² core are indistinguishable from those given by the Ar core plus pair potential, and are also virtually identical to the FP-LMTO results of Söderlind *et al.* [23]. There is a detectable difference from the FLAPW results of Stixrude *et al.* [20], but this is smaller than the difference from the experimental values, which itself is very small in the pressure range 100 – 300 GPa of main interest in this paper.

A further test concerns the low-temperature coexistence pressure of the b.c.c. and h.c.p. phases, which experimentally is in the range 10 – 15 GPa [47]. The earlier FLAPW and FP-LMTO calculations both gave transition pressures of *ca.* 11 GPa. The present PAW calculations give 10, 12 and 13 GPa for the PAW[Ne]3s², PAW[Ar] and PAW[Ar] + effective pair potential respectively, in reasonable agreement with other values.

Finally, we report our comparison of phonon frequencies of the high-pressure non-magnetic f.c.c. phase with the FP-LMTO calculations of Söderlind *et al.* [23]. Frequencies were computed at the three volumes and four wavevectors studied in the FP-LMTO work, and their values are compared in Table II. We note that this is not a very direct comparison, since the FP-LMTO calculations were based on the LDA rather than the GGA used here. We have shown elsewhere [21] that the frequencies of f.c.c. Fe increase slightly when LDA is replaced by GGA, and this is consistent with the difference shown in the Table. However, the differences are no more than a few percent. We also note that the PAW frequencies obtained with the Ar core plus pair potential are almost identical to those given by the Ne3s² core, the effect of the pair potential is to increase the frequencies by 5-10%. This is useful evidence that the procedure of using the Ar core plus pair potential gives a good account of vibrational as well as equilibrium properties.

Our overall conclusion from these tests is that our present PAW calculations appear to reproduce very accurately the properties of real crystalline Fe, and the differences from pseudopotential and standard all-electron implementations of DFT are extremely small. This provides a firm foundation for our PAW simulations of liquid Fe presented in the next Section.

IV. LIQUID IRON

A. A representative *ab initio* simulation

For orientation purposes, we present first the results obtained from a direct *ab initio* simulation of liquid iron at the temperature $T = 4300$ K and the density $\rho = 10700$ kg m⁻³, which corresponds roughly to conditions at the core-mantle boundary. This simulation was

performed on a system of 67 atoms, and used Γ -point sampling. The system was initiated and thoroughly equilibrated in a way that will be described below. The duration of the simulation after equilibration was 15 ps. The pressure was calculated in the course of the simulation and its value was 132 GPa, which should be compared with the value 135 GPa at the core-mantle boundary.

The radial distribution function $g(r)$ from this simulation is displayed in Fig. 3. It shows the form typical of real and theoretical simple liquids such as liquid aluminum or the Lennard-Jones liquid. It is instructive to calculate the average coordination number N_c characterising the number of nearest neighbours surrounding each atom. This is defined as:

$$N_c = 4\pi n \int_0^{r_c} dr r^2 g(r), \quad (1)$$

where n is the atomic number density and r_c is the position of the first minimum in $g(r)$. We find the value $N_c = 13.2$. This is actually slightly greater than the coordination number of 12 exhibited by the close-packed h.c.p. and f.c.c. structures, and it is clear that the liquid structure displays a very dense form of packing. We note that by no means all monatomic liquids show this high coordination. Directionally bonded liquids such as *l*-Se and *l*-Si have very much lower coordination numbers ($N_c \simeq 2$ and 6 in these two cases). The high value of N_c we find for high-pressure *l*-Fe is evidence of strong repulsive forces between the atoms and a complete absence of directional bonding. This is, of course, not surprising given the very high degree of compression.

We now pass to the self-diffusion coefficient D , which we obtain from the asymptotic slope of the time-dependent mean-square displacement (MSD) $\langle |\mathbf{r}_i(t + t_0) - \mathbf{r}_i(t_0)|^2 \rangle$:

$$P(t) = \langle |\mathbf{r}_i(t + t_0) - \mathbf{r}_i(t_0)|^2 \rangle \rightarrow 6D |t| \quad (2)$$

in the long-time limit $|t| \rightarrow \infty$. The quantity $P(t)/6t$ from our simulation is reported in Fig. 4. We also report in the Figure the statistical errors on the MSD, which we shall need to refer to later; these errors were estimated by calculating the MSD separately for every atom in the system and examining the scatter of the results. As generally happens in simple liquids, the asymptotic linear region in the MSD is attained extremely quickly, after a transient period of only ~ 0.3 ps. The asymptotic slope gives the value $D = (5.2 \pm 0.2) \times 10^{-9}$ m² s⁻¹. The value of D is quite typical of simple liquids under ambient conditions. For example, the diffusion coefficient of liquid Al near its triple point [48] is $\sim 8 \times 10^{-9}$ m² s⁻¹. This indicates that the dynamics of the atoms in *l*-Fe under the present thermodynamic conditions is not drastically affected by the high degree of compression.

The final quantity we examine is the shear viscosity η . In our earlier work [24], we relied on the Stokes-Einstein relation to give a rough estimate of the viscosity,

but we subsequently showed that this indirect method is completely unnecessary, since the direct, rigorous calculation of η using the Green-Kubo relation is perfectly feasible [30]. According to this relation, η is given by:

$$\eta = \frac{V}{k_B T} \int_0^\infty dt \langle P_{xy}(t) P_{xy}(0) \rangle, \quad (3)$$

where $\langle P_{xy}(t) P_{xy}(0) \rangle$ is the stress autocorrelation function (SACF), i.e. the autocorrelation function of the off-diagonal component P_{xy} of the stress tensor at times separated by t , and V is the volume of the system. Techniques for calculating the SACF are presented in Ref. [30], where it is noted that statistical accuracy is improved by taking the average $\phi(t)$ of the five independent correlation functions of the traceless stress tensor P_{xy} , P_{yz} , P_{zx} , $\frac{1}{2}(P_{xx} - P_{yy})$ and $\frac{1}{2}(P_{yy} - P_{zz})$.

The average SACF $\phi(t)$ and its time-integral $\int_0^t dt' \phi(t')$ for the present thermodynamic state are reported in Fig. 5, with error bars for the time integral. We obtain from this the value $\eta = 8.5 \pm 1$ mPa s. It is interesting to compare this with the value that would be obtained from the Stokes-Einstein relation:

$$D\eta = k_B T / 2\pi a, \quad (4)$$

where a is an effective atomic diameter. In our previous work, we took the effective atomic diameter a to be the nearest-neighbour distance in the close-packed solid having the same density, which in the present case is 2.15 Å. Using the value $D = 5.2 \times 10^{-9}$ m²s⁻¹ reported above, we obtain the estimate $\eta = 8.5$ mPa s, which happens to be the same as the Green-Kubo value.

Useful though they are, the results we have just presented are limited in two ways. First, there are technical limitations. Our results have been obtained from a rather small simulated system of only 67 atoms, and we must clearly try to show that they are not seriously influenced by size effects. Similarly, we need to know that the results are not affected by other technical factors, such as the use of Γ -point sampling, the choice of the PAW technique rather than some other *ab initio* technique, or the split that we have chosen between valence and core states. The second limitation is that we have studied only one thermodynamic state. We want to know how the properties of *l*-Fe vary over the range of conditions relevant to the Earth's core. In overcoming both these kinds of limitation, the notion of a reference system will be very important, and we discuss this next.

B. The reference system

Since *ab initio* simulation is very costly, it is difficult to study size effects by directly simulating large systems. This is particularly difficult for dynamical properties like the diffusion coefficient and the viscosity, since rather

long simulations are needed. It will be therefore very helpful to have available a simple model or reference system which closely mimics the behaviour of the full *ab initio* system. We have in mind a model in which the atoms interact through a simple pairwise potential $\phi(r)$, so that its total potential energy U_0 is given by:

$$U_0 = \frac{1}{2} \sum_{i \neq j} \phi(|\mathbf{r}_i - \mathbf{r}_j|). \quad (5)$$

If the reference system is to behave like the *ab initio* system, then its total energy U_0 must closely resemble the *ab initio* total energy U . This means that the difference $\Delta U \equiv U - U_0$ must be small. In fact, the requirement is slightly weaker than this. It makes no difference to the thermal-equilibrium structure or dynamics of the liquid if we add a constant to the total energy. So the requirement is really that the *fluctuations* of ΔU should be small. We do not need to demand that the strength of these fluctuations be small over the whole of configuration space. It suffices that they are small over the region explored by the atoms. Regions of configuration space rarely visited by the system should be given a low weighting in assessing the fluctuations, and the natural way to do this is to weight configurations with the Boltzmann factor $\exp[-\beta U(\mathbf{r}_1, \dots, \mathbf{r}_N)]$. The requirement is therefore that the thermal average of the mean-square fluctuations of ΔU defined by $\langle (\Delta U - \langle \Delta U \rangle)^2 \rangle$ be as small as possible. Here, the thermal average $\langle \cdot \rangle$ can be evaluated as a time average over configurations generated in the *ab initio* simulation. It will be noted that this requirement depends on thermodynamic state, so that the best model system may be different for different states.

We have every reason to expect that our *ab initio* liquid can be well modelled by a simple reference system, since we have seen that its properties closely resemble those of typical simple liquids. Initially, we attempted to use the Lennard-Jones model, in which $\phi(r) = 4\epsilon((\sigma/r)^{12} - (r/\sigma)^6)$, where σ and ϵ characterise the atomic diameter and the depth of the attractive potential well respectively. We found that it is possible to choose σ and ϵ so that the fluctuations $\delta\Delta U \equiv \Delta U - \langle \Delta U \rangle$ are reasonably small: the minimum rms value that we achieved was $[\langle (\delta\Delta U)^2 \rangle / N]^{1/2} = 0.18$ eV (N is the total number of atoms in the system). However, the rdf of the resulting LJ liquid differs appreciably from that of the *ab initio* system. Further experimentation showed that a far better reference system is provided by a pure inverse-power potential $\phi(r) = B/r^\alpha$. After adjusting the parameters B and α so as to minimise the strength of the fluctuations $\delta\Delta U$, we achieved a much improved rms value $[\langle (\delta\Delta U)^2 \rangle / N]^{1/2}$ equal to 0.08 eV. Bearing in mind that $k_B T = 0.37$ eV at the temperature of interest, this represents a very satisfactory fit to the *ab initio* system. The resulting value of the exponent α is 5.86, and B is such that for $r = 2$ Å the potential $\phi(r)$ is 1.95 eV.

The inverse-power reference system is so close to the *ab initio* system that its rdf $g_0(r)$ is almost indistinguishable from the rdf of the *ab initio* system. (Naturally, in making this comparison, we treat the two systems at exactly the same thermodynamic state and using the same 67-atom repeating cell.) To show this, we plot the difference $\Delta g(r) \equiv g(r) - g_0(r)$ in Fig. 3. The first peak has almost exactly the same height in the two cases, and the first minimum is also virtually identical; the difference of the two rdfs consists mainly of a slight shift of the first peak of the reference-system to a smaller radius.

Since the reference system is so good, we should expect it to reproduce also the dynamics of the *ab initio* system. To test this, we compare in Fig. 4 the msd of the reference system with the *ab initio* results, using again the 67-atom repeating system. The two curves agree very closely for short times, but there is a significant difference for $t > 0.1$ ps, which is well outside the statistical errors. The diffusion coefficients obtained for PAW and the reference model are 5.2×10^{-9} and 6.1×10^{-9} m^2s^{-1} respectively. Given that the peak position of $g(r)$ is at a slightly smaller radius for the reference model, it is perhaps surprising that the model makes the atoms more mobile, but one should remember that the rdf describes only 2-body correlations, and higher correlations may well be important for diffusion.

Finally, we make the same comparisons for the stress-stress correlation function and its time integral (see Fig. 5). The asymptotic value of the viscosity integral is significantly smaller for the reference model – as one would expect from the higher diffusion coefficient in this case. The *ab initio* and reference viscosities are 8.5 and 7.0 mPa s respectively, so that they differ by *ca.* 20 %, as would be expected from the Stokes-Einstein relation.

Our overall conclusion from these comparisons is that the simple inverse-power reference system with appropriately chosen parameters reproduces the structure of the *ab initio* liquid very well and its dynamics reasonably well. It will be asked whether the same reference system also works for other thermodynamic states, or whether the parameters B and α have to be refitted for every state. This question will be answered in Sec. IV E.

C. Size effects

As an aid to addressing size effects, we have performed a number of *ab initio* simulations at the same thermodynamic state as before ($T = 4300$ K, $\rho = 10700$ kgm^{-3}), using cell sizes ranging from 89 to 241 atoms. The preparation and equilibration of these systems were done using the inverse-power reference system. Since the latter so closely mimics the *ab initio* system for the 67-atom cell, it should provide a well equilibrated starting point for *ab initio* simulation of larger systems. The duration of all the *ab initio* simulations after equilibration was 1 ps.

A duration of 1 ps is enough to give excellent statistical accuracy for the rdf, so our examination of size effects on $g(r)$ was done using the *ab initio* simulations directly. We find that the dependence of $g(r)$ on system size is so small that it cannot easily be seen on simple plots of $g(r)$. To show these effects, we therefore plot the differences $g_N(r) - g_{N'}(r)$ between the rdfs for different numbers of atoms. These differences are reported in Fig. 6 for (N, N') equal to (127, 67) and (241, 127). The difference between $g_{67}(r)$ and $g_{127}(r)$ is small and comes almost entirely in the region of the first peak; the same is true of the difference between $g_{127}(r)$ and $g_{241}(r)$.

We have also looked for size effects by studying how well the inverse-power reference system constructed by fitting to the 67-atom system reproduces the total energy of the larger systems. We find that the rms strength of the fluctuations $[\langle(\delta\Delta U)^2\rangle/N]^{1/2}$ observed in the 1 ps *ab initio* simulations for the larger systems is essentially the same as what we found for the 67-atom system. This confirms that the reference system mimics the large *ab initio* systems as well as it mimics the small one.

A duration of 1 ps is too short to study size effects on D and η directly from the *ab initio* simulations: comparisons between results for different system sizes would be vitiated by statistical noise. However, since the reference model appears to work equally well for all system sizes, we can legitimately use this model to study size effects. We have therefore calculated D and η from simulations of the reference model, using simulations lasting for 500 ps after equilibration. The results are reported in Table III. We note that D increases slightly as we go to larger systems. The effect of system size on D in hard-sphere systems was studied by Erpenbeck and Wood [49], who showed that the calculation of D with 64 atoms would underestimate its value by *ca.* 20%. This is in the same direction as the effect we are seeing, but in our case the error appear to be less than 10%. According to the Stoke-Einstein relation, we would expect a decrease of η with increasing system size, but this is not clear from our results.

D. Other technical factors

We made tests to assess the influence of Brillouin-zone sampling. Since *ab initio* simulations using many k -points are very demanding, we have adopted an indirect approach. Instead of performing direct *ab initio* simulations with many k -points, we have drawn sets of atomic positions $\{\mathbf{r}_i\}$ from the Γ -point simulation, and calculated the total energy U_P with 4 MP k -points for these configurations. We then compute the rms strength of the fluctuations $[\langle(\delta\Delta U_P)^2\rangle/N]^{1/2}$, where $\delta\Delta U_P$ denotes the fluctuation $U_P - U_1 - \langle U_P - U_1 \rangle$, with U_1 the Γ -point energy. This rms fluctuation strength is 0.02 eV, which is much smaller than the rms fluctuation between

the *ab-initio* (Γ -point) system and the reference system. This implies that the expected error in D and η would be barely noticeable, certainly smaller than the statistical errors on these quantities.

In order to test the reliability of using the Ar core plus effective pair potential (see Sec. II), we did a simulation of the liquid at the same thermodynamic state as before, but with the $\text{Ne}3s^2$ core. The duration of this simulation was 4.5 ps. The rdf for this simulation was almost identical to that obtained with the Ar core, the difference being somewhat smaller than the size-effect difference between $g(r)$ for 67 and 127 atoms discussed above. Finally, we have compared $g(r)$ obtained in the present PAW simulations with the one given by our earlier simulations [21] at the same thermodynamic state, which were based on ultrasoft pseudopotentials. Here again, the difference is no bigger than the size effect between 67 and 127 atoms.

Our conclusion from these tests is that our simulations are completely robust with respect to size effects, k -point sampling, the split between valence and core states, and the use of PAW rather than the pseudopotential approach.

E. Dependence of liquid properties on thermodynamic state

In addition to the simulations reported in Sec. IV A, we have also performed PAW simulations at the 15 thermodynamic states listed in Table IV, all these simulations being done on the 67-atom system. With these simulations, we cover the temperature range 3000 – 8000 K and the pressure range 60 – 390 GPa, so that we more than cover the range of interest for the Earth’s liquid core. The Table reports a comparison of the pressures calculated in the simulations with the pressures deduced by Anderson and Ahrens [50] from a conflation of experimental data. Our first-principles pressures reproduce the experimental values to within 2 – 3 % at low densities, but they are systematically too high by *ca.* 7 % at high densities. It is not clear yet whether the high-density discrepancies indicate a real deficiency in the *ab initio* calculations rather than problems in the interpretation of the experimental data. We are currently using free-energy calculations to study the thermodynamics of the liquid in more detail, and we hope that this will shed light on the question.

Rather than reporting detailed results for $g(r)$, D and η at each thermodynamic state, we can exploit the properties of the reference system to present the results in a compact form. We have taken the reference system fitted to the *ab initio* simulations at $T = 4300$ K and $\rho = 10700$ kg m⁻³, and examined the fluctuations $\delta\Delta U$ in the *ab initio* simulations done at the other thermodynamic states. We find that the strength of the fluctuations is not significantly greater for these other states than it was for the state for which the model was fitted.

This strongly indicates the same reference model, with exactly the same parameters, mimics the first-principles system (almost) equally well at all thermodynamic states.

The invariance of the reference system implies a truly remarkable simplicity in the variation of the liquid properties with thermodynamic state. It has long been recognised that the properties of an inverse-power system in thermal equilibrium depend non-trivially only on a single thermodynamic variable, rather than on temperature T and number density n independently [51]. This variable is:

$$\zeta = Bn^{\alpha/3}/k_B T. \quad (6)$$

Any other dimensionless combination of the parameters B , T and n is a function only of ζ . This means, for example, that the rdf $g(r)$, since it is dimensionless, can depend only on ζ , provided it is regarded as a function of the dimensionless distance $\xi \equiv n^{1/3}r$. To formulate this statement precisely, let us define the ‘reduced’ rdf $\bar{g}(\xi)$ as:

$$\bar{g}(n^{1/3}r) = g(r). \quad (7)$$

Then $\bar{g}(\xi)$ must be a function only of ζ . Similarly, the reduced diffusion coefficient \bar{D} and viscosity $\bar{\eta}$, defined by:

$$\bar{D} = (m/k_B T)^{1/2} n^{1/3} D, \quad \bar{\eta} = (mk_B T)^{-1/2} n^{-2/3} \eta \quad (8)$$

can depend only on ζ .

To show the ζ -dependence of the rdf, we report in Fig. 7 the rdf $g(r)$ for the five temperatures 4300, 5000, 6000, 7000 and 8000 K at the same density $\rho = 10700$ kg m⁻³; the corresponding values of ζ are 4.51, 3.88, 3.23, 2.77 and 2.43. The effect of varying temperature (or ζ) is clearly not dramatic, and consists of the expected weakening and broadening of the structure with increasing T . Since the variation is so regular, we can obtain $\bar{g}(\xi)$ for any intermediate value of ζ by simple linear interpolation between the curves. With this information, we can then test explicitly our expectation that $\bar{g}(\xi)$ depends only on ζ . To do this, we go to states at other densities ρ and compare the reduced rdf with the $\bar{g}(\xi)$ for the same ζ but for the density $\rho = 10700$ kg m⁻³. We find that the agreement is excellent; indeed, the differences between $\bar{g}(\xi)$ at the same ζ but different density are even smaller than those between $g(r)$ for *ab initio* and reference model discussed in Sec. IV A. This shows that the rdf for any thermodynamic state in the range we have studied can be obtained directly from the results shown in Fig. 7.

Since most of the simulations reported in Table V are rather short – typically no more than 4 ps – the statistical accuracy on D and η is not great. Numerical results, together with error estimates obtained as in Sec. IV A,

are reported in Table V. If the reduced quantities \bar{D} and $\bar{\eta}$ defined in eqn (8) depend only on ζ , then a plot of \bar{D} against ζ should consist of a single curve, and similarly for $\bar{\eta}$. This hypothesis is tested in Fig. 8, and appears to be satisfied within the (significant) errors. This means that the diffusion coefficient and viscosity at any thermodynamic state in the range we have studied can be deduced from the data in Fig. 8.

V. DISCUSSION AND CONCLUSIONS

The *ab initio* simulations we have presented demonstrate that under Earth’s core conditions *l*-Fe is typical simple liquid. In common with other simple liquids like *l*-Ar and *l*-Al, it has a close-packed structure, the coordination number in the present case being *ca.* 13. For the entire pressure-temperature domain of interest for the Earth’s outer core, the diffusion coefficient D and viscosity η are comparable with those of typical simple liquids, D being *ca.* $5 \times 10^{-9} \text{ m}^2\text{s}^{-1}$ and η being in the range 8 – 15 mPa s, depending on the detailed thermodynamic state.

We have shown that the structural properties of *l*-Fe are reproduced very accurately and the dynamical properties fairly accurately by an inverse-power model, and consequently that they display a remarkable scaling property. Instead of depending on T and n separately, their only non-trivial dependence is on the combined thermodynamic variable ζ discussed in Sec. IV E. Since the Earth’s outer core is in a state of convection, the temperature and density will lie on adiabats. It is straightforward to show that the variation of ζ along adiabats will be rather weak. For example, if we take the data for high-pressure liquid iron compiled by Anderson and Ahrens [50], then the adiabat for $T = 6000 \text{ K}$ at the ICB pressure 330 GPa has $T = 4300 \text{ K}$ at the CMB pressure of 135 GPa. Taking the densities at these two points from the same source, we find values of ζ equal to 4.85 and 4.51 at the ICB and CMB respectively. Fig. 7 shows that this small variation of ζ leaves the liquid structure virtually unchanged, apart from a trivial length scaling. For all practical purposes, then, it can be assumed that variation of thermodynamic conditions across the range found in the core has almost no effect on the liquid structure. For the same reasons, the reduced diffusion coefficient \bar{D} and viscosity $\bar{\eta}$ also show little variation. From the results reported in Sec. IV E, it is readily shown that the true (unreduced) diffusion coefficient D is $5 \pm 0.5 \times 10^{-9} \text{ m}^2\text{s}^{-1}$ without significant variation as one goes from ICB to CMB pressures along the above-mentioned adiabat, and η goes from $15 \pm 5 \text{ mPa s}$ to $8.5 \pm 1 \text{ mPa s}$ along this adiabat.

We have made strenuous efforts to demonstrate the robustness and reliability of the calculations. Our results

on the solid show that the predictions from our pseudopotential and PAW *ab initio* techniques agree very closely both with experiment and with the results of other all-electron calculations. This is true both at ambient pressures and at Earth’s core pressures. For the liquid, we have shown that our results are completely robust with respect to all the main technical factors: size of simulated system, k -point sampling, choice of *ab initio* method and split between core and valence states. At present, *ab initio* dynamical simulations of the type presented here are only practicable with the PAW or pseudopotential techniques. However, our comparisons leave little doubt that if such simulations were feasible with other DFT techniques, such as FLAPW, virtually identical results would be obtained. In addition, we have been able to compare the calculated pressure in the liquid with values deduced from experiments, and again the good agreement supports the validity of our techniques.

Finally, we note the implications of this work for the controversy about the viscosity of the Earth’s core. In our earlier work on this problem, we presented *ab initio* simulations on a 64-atom system and used results for the diffusion coefficient together with the Stokes-Einstein relation to argue that the viscosity of pure *l*-Fe under core conditions is *ca.* 13 mPa s. Although we regarded this prediction as sound, it was certainly open to the objection that the simulated system was too small, and that the viscosity was inferred indirectly. We believe that the present work has completely overcome both these objections, as well as giving results for the viscosity over a wide range of conditions. We fully confirm our earlier conclusion that the viscosity of pure liquid iron under Earth’s core conditions is at the lower end of the range of proposed values.

In conclusion, *l*-Fe under Earth’s core conditions is a simple liquid with a close-packed structure and a coordination number of 13, and a viscosity going from 15 mPa s to 8 mPa s as conditions go from the the inner-core boundary to the core-mantle boundary. These results are completely robust with respect to system-size effects, choice of *ab initio* method, and other technical factors.

ACKNOWLEDGMENTS

The work of DA was supported by NERC grant GST/O2/1454 to G. D. Price and M. J. Gillan, and the work of GK by EPSRC grant GR/L08946. Allocations of time on the Cray T3E machines at the Manchester CSAR service and at Edinburgh Parallel Computer Centre was provided through the UK Car-Parrinello consortium and the Minerals Physics consortium.

- [1] F. Birch, *Geophys. Res.* **57**, 227 (1952).
- [2] D. L. Anderson, *Theory of Earth* (Blackwell Scientific Publications, London, 1989).
- [3] J.-P. Poirier, *Introduction to the Physics of the Earth's Interior* (Cambridge University Press, 1991).
- [4] O. L. Anderson and A. Duba, *J. Geophys. Res.* **102**, 22659 (1997).
- [5] Q. Williams, R. Jeanloz, J. Bass, B. Svendsen and T. J. Ahrens, *Science*, **236**, 181 (1987).
- [6] R. Boehler, N. von Bargen and A. Chopelas, *J. Geophys. Res.* **95**, 21731 (1990).
- [7] R. Boehler, *Nature*, **363**, 534 (1993).
- [8] D. Andrault, G. Fiquet, M. Kunz, J. Visocekas, D. Häusermann, *Science* **278**, 831 (1997).
- [9] G. Shen, H. Mao, R. J. Hemley, T. S. Duffy and M. L. Rivers, *Geophys. Res. Lett.* **25**, 373 (1998).
- [10] R. Jeanloz, *J. Geophys. Res.*, **84**, 6059 (1979).
- [11] J. M. Brown and R. G. McQueen, *J. Geophys. Res.* **91**, 7485 (1986).
- [12] J. D. Bass, B. Svendsen, and T. J. Ahrens, in *High Pressure Research in Mineral Physics*, *Geophys. Monogr. Ser.* **39**, edited by M. H. Manghnani and Y. Syono, 393-492 (American Geophysical Union Washington, D. C., 1987).
- [13] R. A. Secco, in *Mineral Physics and Crystallography: A Handbook of Physical Constants* (ed. T. J. Ahrens), 218 (American Geophysical Union, 1995).
- [14] V. V. Brazhkin, *JETP Lett.*, **68**, 502 (1998).
- [15] D. P. Dobson, A. P. Jones, R. Rabe, T. Sekine, K. Kurita, T. Taniguchi, T. Kondo, T. Kato, O. Shimomura and S. Urakawa, *Earth Planet. Sci. Lett.*, **143**, 207 (1996).
- [16] G. E. Le Blanc and R. A. Secco, *Geophys. Res. Lett.*, **23**, 213 (1996).
- [17] R. Car and M. Parrinello, *Phys. Rev. Lett.*, **55**, 2471 (1985).
- [18] R. O. Jones and O. Gunnarsson, *Rev. Mod. Phys.* **61**, 689 (1989).
- [19] M. J. Gillan, *Contemp. Phys.*, **38**, 115 (1997).
- [20] L. Stixrude, R. E. Cohen and D. J. Singh, *Phys. Rev. B*, **50**, 6442 (1994).
- [21] L. Vočadlo, G. A. de Wijs, G. Kresse, M. Gillan and G. D. Price, *Faraday Disc.*, **106**, 205 (1997).
- [22] L. Vočadlo, J. Brodholt, D. Alfè, M. J. Gillan and G. D. Price, *Phys. Earth Planet. Interiors*, in press.
- [23] P. Söderlind, J. A. Moriarty and J. M. Willis, *Phys. Rev. B*, **53**, 14063 (1996).
- [24] G. A. de Wijs, G. Kresse, L. Vočadlo, D. Dobson, D. Alfè, M. J. Gillan and G. D. Price, *Nature*, **392**, 805 (1998).
- [25] D. Alfè and M. J. Gillan, *Phys. Rev. B*, **58**, 8248 (1998).
- [26] D. Alfè, G. D. Price and M. J. Gillan, *Phys. Earth Planet. Interiors*, **110**, 191 (1999).
- [27] P. E. Blöchl, *Phys. Rev. B*, **50**, 17953 (1994).
- [28] G. Kresse and D. Joubert, *Phys. Rev. B*, **59**, 1758 (1999).
- [29] S. Wei and H. Krakauer, *Phys. Rev. Lett.*, **55**, 1200 (1985).
- [30] D. Alfè and M. J. Gillan, *Phys. Rev. Lett.*, **81**, 5161 (1998).
- [31] R. G. Parr and W. Yang, *Density-Functional Theory of Atoms and Molecules*, (Oxford University Press, Oxford, 1989).
- [32] M. C. Payne, M. P. Teter, D. C. Allan, T. A. Arias, J. D. Joannopoulos, *Rev. Mod. Phys.* **64**, 1045 (1992).
- [33] P. Hohenberg and W. Kohn, *Phys. Rev.*, **136**, B864 (1964).
- [34] W. Kohn and L. Sham, *Phys. Rev.*, **140**, A1133 (1965).
- [35] N. D. Mermin, *Phys. Rev.*, **137**, A1441 (1965).
- [36] D. Vanderbilt, *Phys. Rev. B*, **41**, 7892 (1990).
- [37] G. Kresse and J. Furthmüller, *Comput. Mater. Sci.*, **6**, 15 (1996).
- [38] G. Kresse and J. Furthmüller, *Phys. Rev. B*, **54**, 11169 (1996).
- [39] P. Ballone, G. Galli, *Phys. Rev. B*, **40**, 8563 (1989).
- [40] Y. Wang and J. Perdew, *Phys. Rev. B*, **44**, 13298 (1991).
- [41] J. P. Perdew, J. A. Chevary, S. H. Vosko, K. A. Jackson, M. R. Pederson, D. J. Singh and C. Fiolhais, *Phys. Rev. B*, **46**, 6671 (1992).
- [42] S. H. Vosko, L. Wilk, and M. Nusair, *Can. J. Phys.*, **58**, 1200 (1980).
- [43] H. J. Monkhorst and J. D. Pack, *Phys. Rev. B*, **13**, 5188 (1976).
- [44] D. Alfè, *Computer Phys. Commun.*, **118**, 31-33 (1999).
- [45] H. K. Mao, Y. Wu, L. C. Chen, J. F. Shu, and A. P. Jephcoat, *J. Geophys. Res.*, **95**, 21737 (1990).
- [46] G. Kresse, J. Furthmüller, and J. Hafner, *Europhys. Lett.* **32**, 729 (1995).
- [47] A. P. Jephcoat, H. K. Mao, and P. M. Bell, *J. Geophys. Res.* **91**, 4677 (1986).
- [48] *CRC Handbook of Chemistry and Physics*, Editor D. R. Lide, 74th edition (1993).
- [49] J. J. Erpenbeck and W. W. Wood, *Phys. Rev. A*, **32**, 412 (1985).
- [50] W. W. Anderson and A. T. J. Ahrens, *J. Geophys. Res.* **99**, 4273 (1994).
- [51] W. G. Hoover, S. G. Gray, and K. W. Johnson, *J. Chem. Phys.*, **55**, 1128 (1971).
- [52] E. Knittle, in *Mineral Physics and Crystallography: A Handbook of physical constants*, ed. T. J. Ahrens, (American Geophysical Union, Washington, p. 131, 1995).
- [53] G. G. Lonzarich, *Electrons at the Fermi Surface*, ed. M. Springford, Cambridge University Press, Cambridge, p.225 (1980).
- [54] B. N. Brockhouse, H. E. Abou-Helal, E. D. Hallman, *Solid State Commun.*, **5**, 211 (1967).

		V_0 (\AA^3)	K_0 (GPa)	K'_0	μ/μ_B
b.c.c.	PAW [Ne]3s ²	11.51	178	4.8	2.22
	PAW [Ar]	11.47	176	4.8	2.23
	PAW [Ar] + corr	11.53	176	4.8	
	USPP [Ne]3s ²	11.63	181	4.6	2.25
	USPP [Ar]	11.74	167	4.7	2.32
	USPP [Ar] + corr	11.78	163	4.7	
	FLAPW	11.39	189	4.9	2.17
	expt.	11.80	162 – 176	5.0	2.12
h.c.p.	PAW [Ne]3s ²	10.25	287	4.5	
	PAW [Ar]	10.19	289	4.5	
	PAW [Ar] + corr	10.26	288	4.5	
	USPP [Ne]3s ²	10.35	291	4.4	
	USPP [Ar]	10.32	281	4.2	
	USPP [Ar] + corr	10.38	296	4.2	
	FLAPW	10.20	291	4.4	
	expt.	11.2	208		

TABLE I. Properties of the b.c.c. and h.c.p. crystal structures of Fe at zero pressure obtained in the present PAW and USPP calculations compared with FLAPW and experimental values. Properties reported are: the equilibrium volume per atom V_0 , the bulk modulus K_0 , the pressure derivative $K'_0 \equiv dK_0/dp$ and the magnetic moment μ per atom (units of Bohr magneton μ_B). FLAPW results are those of Ref. [20]. Experimental results all come from Ref. [52], except for μ , which comes from Ref. [53].

V_0 (\AA^3)		L[100]	T[100]	L[111]	T[111]
6.17	FP-LMTO	19.6	13.6	22.0	9.56
	PAW [Ne]3s ²	20.4	14.0	22.9	9.61
	PAW [Ar]+corr	20.2	13.7	22.9	9.42
7.55	FP-LMTO	13.4	10.1	15.9	7.19
	PAW [Ne]	14.2	10.5	16.4	7.16
	PAW [Ar]+corr	14.0	10.3	16.4	7.15
9.70	FP-LMTO	6.33	6.37	8.93	4.89
	PAW [Ne]3s ²	7.23	6.43	9.52	4.65
	PAW [Ar]+corr	7.35	6.49	9.64	4.74

TABLE II. Zone boundary phonon frequencies (THz units) of f.c.c. Fe from the present PAW calculations compared with the FP-LMTO results of Ref. [23]. Results are shown for three values of the volume per atom V_0 . PAW results are given for both the Ne3s² core and the Ar core plus effective pair-potential correction (see text).

		67	127	241	499
$D(10^{-9} \text{ m}^2 \text{ s}^{-1})$	PAW [Ne]3s ²	4.8 ± 0.2			
	PAW [Ar] + corr	5.2 ± 0.2			
	Ref. model	6.1	6.2	6.4	6.5
η (mPa s)	PAW [Ne]3s ²	5.5 ± 2			
	PAW [Ar] + corr	8.5 ± 1			
	Ref. model	7.0	7.5	7.0	6.5

TABLE III. Comparison of *ab-initio* and reference-model values of the diffusion coefficient D and the viscosity η for simulated *l*-Fe systems containing 67, 127, 241 and 499 atoms at $T = 4300$ K and $\rho = 10700 \text{ kg m}^{-3}$. PAW results are given for the Ne3s² core and the Ar core with pair-potential correction (see text).

T (K)	ρ (kg m^{-3})				
	9540	10700	11010	12130	13300
3000	60				
4300	132				
	(135)				
5000	140				
	(145)				
6000	90	151	170	251	360
		(155)	(170)	(240)	(335)
7000	161				
				(250)	(350)
8000	172				
			191	275	390
	(360)				

TABLE IV. Pressure (GPa units) calculated in the full set of 16 *ab-initio* simulations of *l*-Fe. Experimental values (in parenthesis) are from Ref. [50].

		ρ (kg m^{-3})				
T (K)		9540	10700	11010	12130	13300
$D(10^{-9} \text{ m}^2 \text{ s}^{-1})$	3000	4.0 ± 0.4				
	4300	5.2 ± 0.2				
	5000	7.0 ± 0.7				
	6000	14 ± 1.4	10 ± 1	9 ± 0.9	6 ± 0.6	5 ± 0.5
	7000		13 ± 1.3	11 ± 1.1	9 ± 0.9	6 ± 0.6
η (mPa s)	3000	6 ± 3				
	4300	8.5 ± 1				
	5000	6 ± 3				
	6000	2.5 ± 2	5 ± 2	7 ± 3	8 ± 3	15 ± 5
	7000		4.5 ± 2	4 ± 2	8 ± 3	10 ± 3

TABLE V. The diffusion coefficient D and the viscosity η from *ab-initio* simulations of *l*-Fe at a range of temperatures and densities. The error estimates come from statistical uncertainty due to the short duration of the simulation.

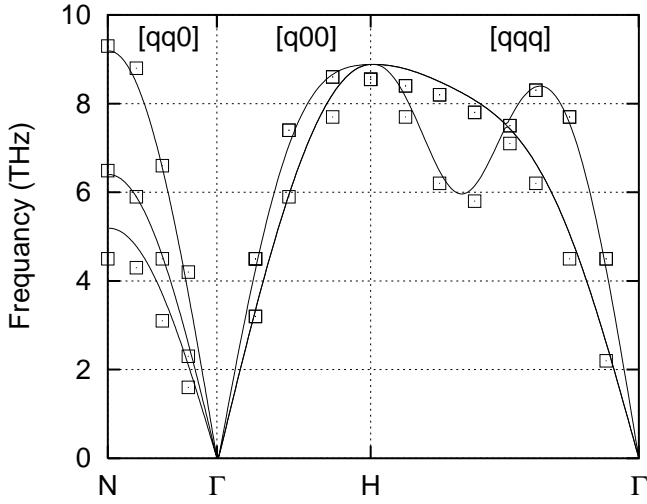


FIG. 1. Phonon dispersion curves of ferromagnetic b.c.c. Fe at zero pressure along the [100], [110] and [111] directions. Curves show calculated phonon frequencies, open squares are experimental data of Ref. [54].

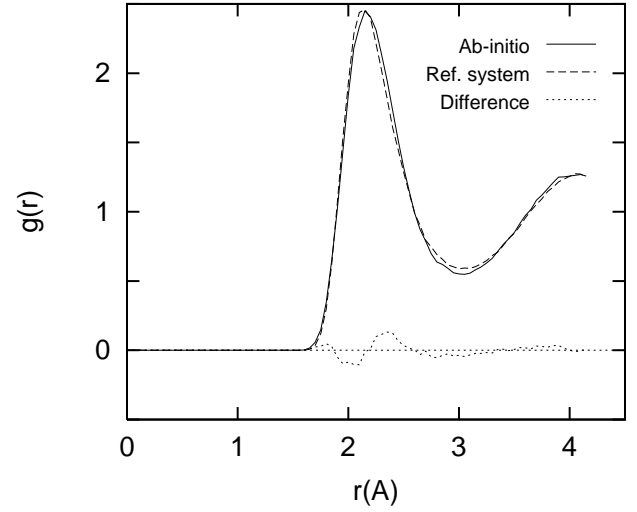


FIG. 3. Radial distribution function $g(r)$ of l -Fe at $T = 4300$ K and $\rho = 10700$ kg m⁻³. Solid and dashed curves are *ab-initio* and reference-model results, dotted curve is the difference of the two.

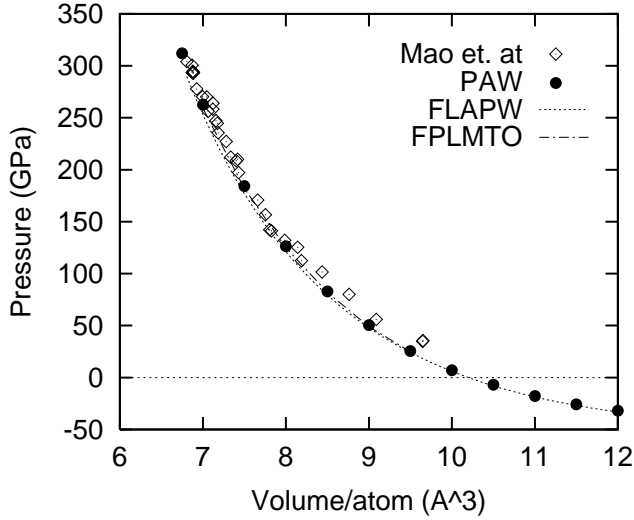


FIG. 2. Pressure as a function of atomic volume of h.c.p. Fe. Solid circles are present PAW calculations; dotted and chain curves are FLAPW and FP-LMTO results of Ref. [20] and [23] respectively, diamonds are experimental values of Ref. [45]

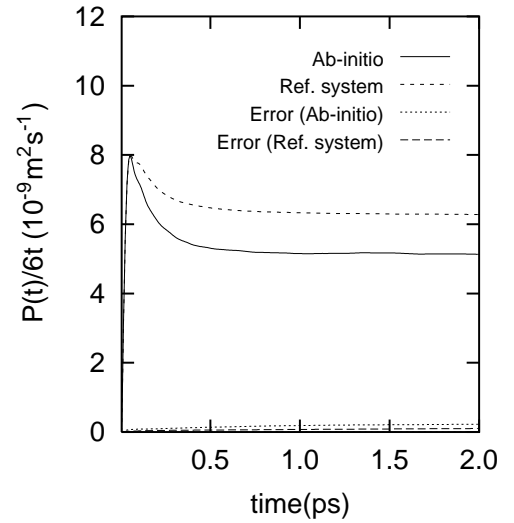


FIG. 4. Mean-square displacement $P(t)$ divided by $6t$ for l -Fe at $T = 4300$ K and $\rho = 10700$ kg m⁻³. Solid and short-dashed curves show results for *ab-initio* and reference system, with statistical error shown as dots and long dashes.

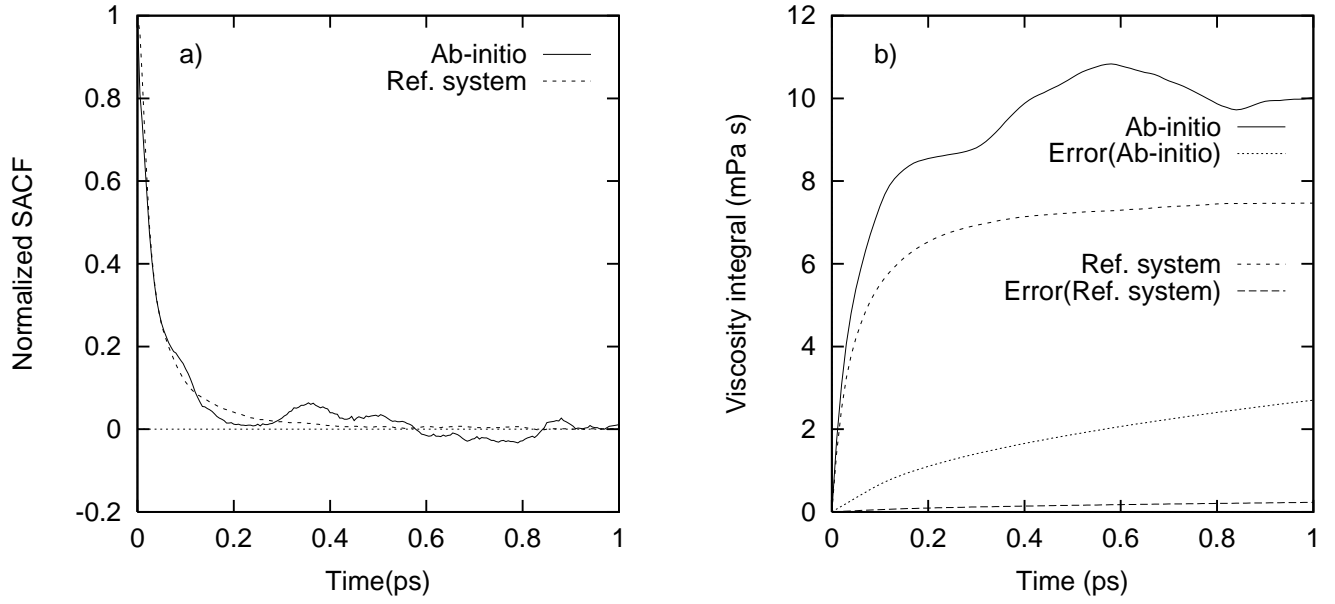


FIG. 5. (a) Stress autocorrelation function (see eqn. (3)) normalised to its $t = 0$ value of liquid Fe at $T = 4300$ K and $\rho = 10700$ kg m $^{-3}$. Solid and short-dashed curves show *ab-initio* and reference-system results. (b) Viscosity integral (see text) of *l*-Fe at the same thermodynamic state. Solid and short-dashed curves as in panel (a); dotted and long-dashed curves show statistical errors.

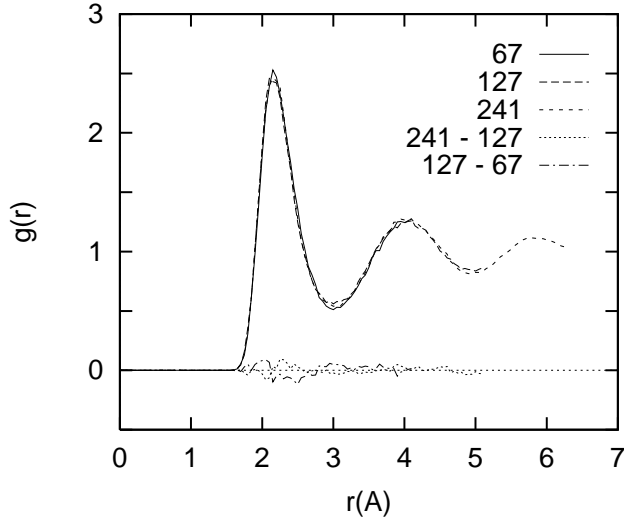


FIG. 6. Comparison of radial distribution function $g(r)$ from *ab-initio* simulations of *l*-Fe using different system sizes. Solid, long-dash and short-dash curves show $g(r)$ for systems of 67, 127 and 241 atoms; dotted and chain curves show differences $g_N(r) - g_{N'}$ for (N, N') equal to (127,67) and (241,127) respectively.

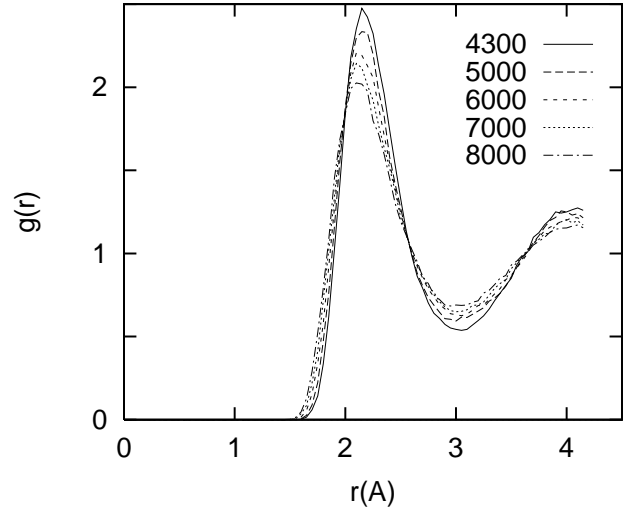


FIG. 7. Variation of $g(r)$ with temperature from *ab-initio* simulations of *l*-Fe at the fixed density $\rho = 10700$ kg m $^{-3}$. Results are shown for the five temperatures $T = 4300, 5000, 6000, 7000$ and 8000 K.

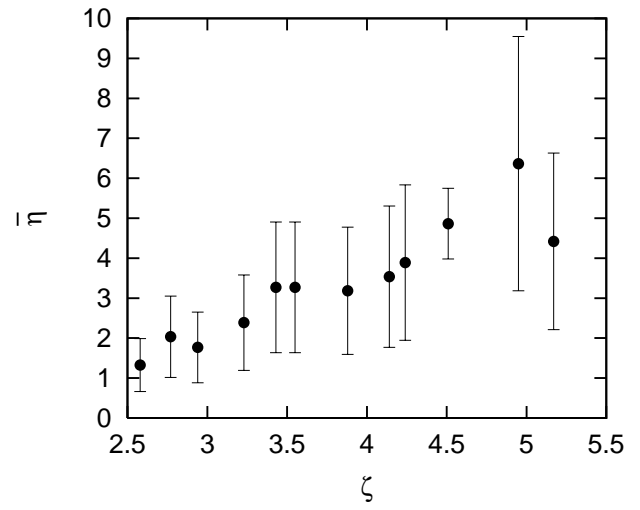
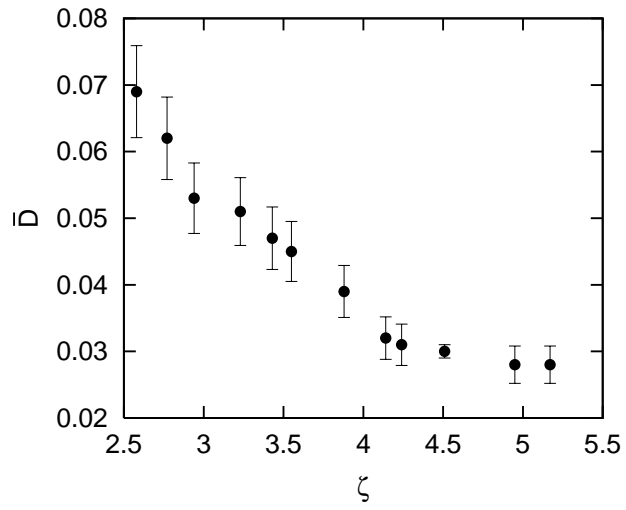


FIG. 8. Reduced diffusion coefficient \bar{D} and viscosity $\bar{\eta}$ as a function of reduced state variable ζ (see text) from ab-initio simulations of l -Fe at 12 thermodynamic states. Error bars show statistical uncertainty on each point.